The Astrophysical Journal, 945:151 (7pp), 2023 March 10 https://doi.org/10.3847/1538-4357/acbd38

Ambipolar Heating of Magnetars

Sachiko Tsuruta[1,2], Madeline J. Kelly[1], Ken'ichi Nomoto[2], Kanji Mori[3], Marcus Teter[1,4], and Andrew C. Liebmann[1]
[1] Department of Physics, Montana State University, Bozeman, MT 59717, USA
[2] Kavli Institute for the Physics and Mathematics of the Universe (WPI), The University of Tokyo, Kashiwa, Chiba 277-8583, Japan
[3] Research Institute of Stellar Explosive Phenomena, Fukuoka University, 8-19-1 Nakamura, Jonan-ku, Fukuoka, Fukuoka 814-0180, Japan
[4] Raytheon Technologies, 16510 E. Hughes Dr., Aurora, CO 80011, USA
Received 2021 November 11; revised 2023 February 6; accepted 2023 February 9; published 2023 March 16

Abstract

Magnetars, neutron stars thought to be with ultrastrong magnetic fields of $10^{14–15}$ G, are observed to be much hotter than ordinary pulsars with $\sim 10^{12}$ G, and additional heating sources are required. One possibility is heating by the ambipolar diffusion in the stellar core. This scenario is examined by calculating the models using the relativistic thermal evolutionary code without making the isothermal approximation. The results show that this scenario can be consistent with most of the observed magnetar temperature data.

Unified Astronomy Thesaurus concepts: Magnetars (992); X-ray stars (1823); Degenerate matter (367); Neutron stars (1108)

1. Introduction

The soft gamma-ray repeaters and the anomalous X-ray pulsars are now considered to be magnetars, the same population of the ultrastrongly magnetized neutron stars with magnetic fields of the order of 10^{14}–10^{15} G on the surface (e.g., Heyl & Hernquist 1998; Thompson & Duncan 2001; Mereghetti 2008; Potekhin et al. 2015). Activities in these stars are powered by the dissipation of strong magnetic energy (e.g., Thompson & Duncan 2001). Magnetars generally undergo long quiescent periods with persistent X-ray emission between a shorter recurrent phase of gamma-ray bursts (e.g., Mereghetti 2008).

During the quiescent phase the star is in a nearly steady equilibrium state. The surface temperature of many magnetars during this phase has been measured. Figure 1 shows the measured surface luminosity (and hence surface temperature) of magnetars (taken from Viganò et al. 2013), which is compared with theoretical thermal evolution curves for ordinary neutron stars with magnetic fields of 10^{12} G (Tsuruta et al. 2009).

In this figure, two upper thick solid curves are for $1.4M_{\odot}$ neutron stars, with the lower curve for cooling only while the upper one includes the maximum vortex creep heating. Two curves between these thick solid curves show the vortex creep heating with intermediate strength. The hot dashed curve is for stars with crusts contaminated by light elements. The lower three curves represent stars with $1.5M_{\odot}$, $1.6M_{\odot}$, and $1.8M_{\odot}$, respectively, in the order of decreasing luminosity. When the stellar mass reaches $M_{\rm tr} = 1.45M_{\odot}$, the transition from neutron matter to hyperon-mixed matter takes place. Therefore, these are hyperon stars with nonstandard fast cooling. For the intermediate case of the $1.5M_{\odot}$ and $1.6M_{\odot}$ stars, superfluid suppression is effective. However, for the heaviest $1.8M_{\odot}$ star, the central density is so high that the corresponding critical temperature for superfluidity becomes so low that the superfluid suppression disappears.

It is clear that most magnetars are hotter than ordinary neutron stars. The surface temperature becomes higher with stronger magnetic fields, but with cooling alone the temperature can not become as high as the observed magnetar temperatures when the surface magnetic fields are increased even to as high as 10^{15} G (assuming the conventional magnetic field structure, which becomes dipolar globally; e.g., Heyl & Hernquist 1998). With a certain special magnetic field configuration where ultrastrong magnetic fields of as high as $\sim 10^{16}$ G are deposited in the equatorial plane near the inner edge of the inner crusts, the star was shown to become as hot as the observed magnetars (Viganò et al. 2013; Potekhin et al. 2015). However, it was since then pointed out that this special magnetic structure is unlikely to last long due to instability (Beloborodov & Li 2016, hereafter BL16). Therefore, it is important to explore the heating of magnetars with a more conventional magnetic field structure.

In the following, we only consider such a conventional magnetosphere case. There are several possible heating scenarios proposed for magnetars (e.g., BL16; Thompson & Duncan 2001). The star can be heated in the interior, either within the stellar core or in the crustal layers. It can be heated from the outside, from the magnetosphere, also (see Thompson & Duncan 2001, BL16).

Kaminker et al. (2006) considered the crustal heating of magnetars by using their thermal evolution code and explored the effect of the location of the heat source in the crusts and heating rate on the stellar surface temperature. It was concluded that a heating rate of $\sim 3 \times 10^{19}$ erg cm^{-3} s^{-1} is required at depths of 300 m or less to sustain the surface radiation luminosity of 10^{35} erg s^{-1} required for magnetars. These authors, however, did not consider the physical mechanisms for the heating, although some comments were made.

Some other authors considered various heating mechanisms for magnetars (e.g., Thompson & Duncan 2001, BL16). Recently BL16 showed that a variety of heating mechanisms possible in the stellar crusts, such as the Hall effect, ohmic dissipation, etc., will fail to increase the surface temperature to as high as the observed magnetar data.

Recently as one of the possible mechanisms for heating magnetars, BL16 proposed the ambipolar process, which takes

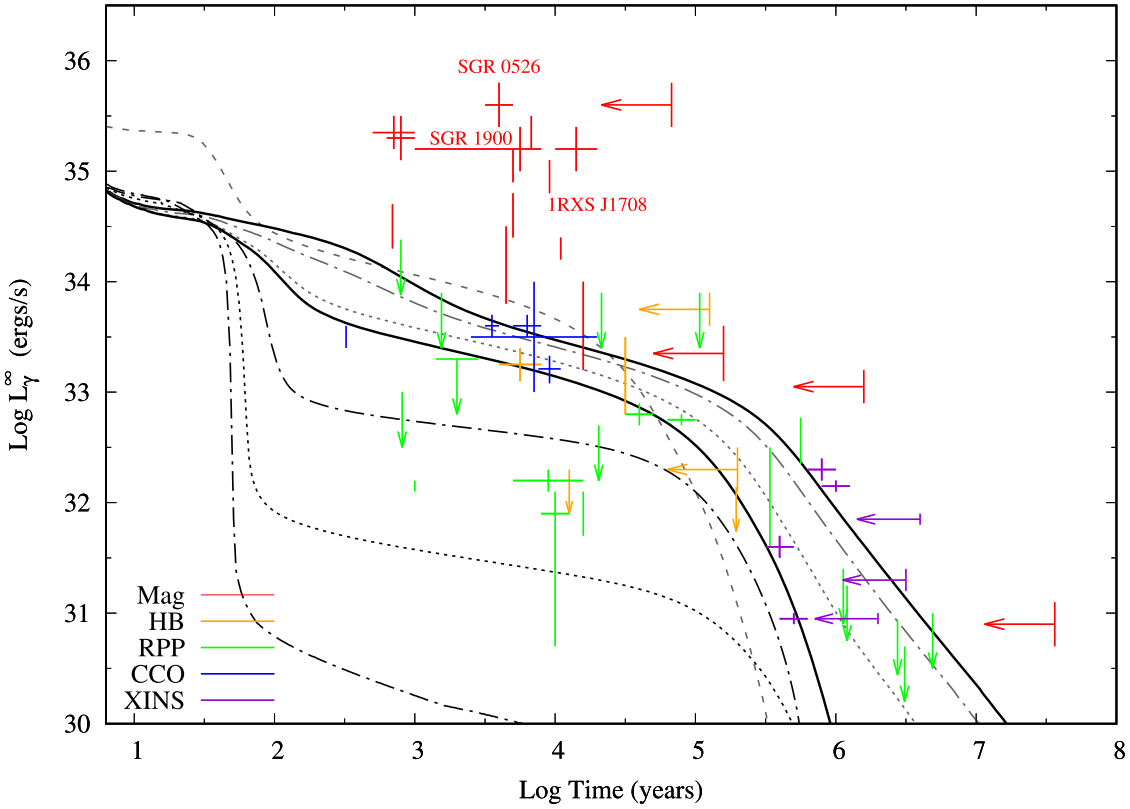

Figure 1. Theoretical thermal evolution curves for various ordinary pulsars are compared with the observed surface photon luminosity (hence surface temperature) data of various kinds of neutron stars taken from Viganò et al. (2013). The observed data points are grouped into five categories. Red are magnetars (Mag), orange are High-B pulsars (HB), green are rotation-powered pulsars (RPP), blue are central compact objects (CCO), and purple are X-ray isolated neutron stars (XINS). The bars and crosses are detections. Arrows pointing down represent upper limits on measured luminosity, and arrows pointing to the left represent upper limits on age. See Viganò et al. (2013) for more complete details.

place in the magnetar's central core. In this process, magnetic energy is dissipated by the ambipolar drift, which is the motion of the electron–proton plasma through the approximately static neutron fluid in the stellar core. The drift is driven by the Lorentz force. The ambipolar diffusion driven by the Lorentz force is opposed by proton–neutron friction and pressure gradients. These authors, however, adopted a simple analytic approach with a Newtonian model for a constant temperature and density core using the isothermal approximation.

Under the isothermal approximation, the core from the center to a certain density ρ_b is isothermal where the timescale of thermal conduction is assumed to be negligible (Tsuruta 1964, 1979). BL16 adopted $\rho_b = 10^9$ g cm^{-3}. Then the cooling and heating effects of each layer are instantaneously transported throughout the core. The thin outer envelope at $\rho < \rho_b$ has a spacially constant luminosity. With this isothermal approximation, the surface luminosity follows the change in the core temperature instantaneously. However, in the early stage of the thermal evolution of the neutron star, the neutrino emission in the core is much faster than the thermal conduction so that the surface luminosity does not necessarily keep pace with the thermal evolution of the core (Nomoto & Tsuruta 1981, 1987).

We will, therefore, investigate this internal heating due to the ambipolar process by fully taking into account the finite timescale of heat conduction in the core. We use the magnetar evolutionary simulation code, which fully includes general relativity (Thorne 1977; Nomoto & Tsuruta 1981, 1987) and realistic stellar physics with the relevant equation of state (EOS).

In Section 2 we review the ambipolar diffusion process and then show how that will heat the stellar interior by the magnetic energy dissipated by this process. Section 3 introduces our physical model and summarizes our method and approach. Section 4 presents the results. The discussion and concluding remarks are given in Sections 5 and 6.

2. Magnetar Heating by Ambipolar Diffusion

2.1. Ambipolar Diffusion Process

The main process capable of dissipating magnetic energy in a magnetar's core is diffusion through ambipolar drift (Goldreich & Reisenegger 1992; Thompson & Duncan 1996). Ambipolar drift is the motion of the electron–positron plasma through the (approximately static) neutron fluid. The drift is driven by the Lorentz force $J \times B/c = (\nabla \times B) \times B/4\pi$ and tends to relieve the magnetic stresses that drive it. The drift is opposed by (i) friction against the neutron fluid and (ii) pressure perturbations it induces. The friction is due to nuclear collisions between neutrons and protons. (Electron–neutron collisions are negligible.)

The rate of proton–neutron collisions per proton, τ_{pn}, is (BL16)

$$\tau_{pn}^{-1} \approx 5 \times 10^{18} T_9^2 (\rho/\rho_{nuc})^{-1/3} Q_{pn} \ \mathrm{s}^{-1}, \quad (1)$$

where T_9 is the temperature in the unit of 10^9 K, ρ is the density, and $\rho_{nuc} \approx 2.8 \times 10^{14}$ g cm^{-3} is the nuclear density. Q_{pn} describes suppression of the rate of collisions among protons and

neutrons. It refers to proton (p) superconductivity and neutron (n) superfluidity. If there exists no proton superconductivity and no neutron superfluidity $Q_{\rm pn}=1$. If they are present, $Q_{\rm pn}<1$ (see Sections 5.2 and 5.3 for the details).

Pressure perturbations are induced if $\nabla\cdot(n_e\boldsymbol{v})\neq 0$, where $n_e=n_{\rm p}$ are the electron (e) and proton (p) number density and $\boldsymbol{v}$ is the proton drift velocity. This compressive drift generates a change in n_e which changes the electron and proton pressures. That is related to the chemical potentials of electron and proton μ_e and $\mu_{\rm p}$. Then the resultant pressure gradient is given as $-n_e\nabla(\Delta\mu)$ where

$$\Delta\mu=\mu_e+\mu_{\rm p}-\mu_{\rm n}. \tag{2}$$

$\mu_{\rm n}$, $\mu_{\rm p}$, and μ_e are, respectively, neutron, proton, and electron chemical potential. Equation (2) describes a local deviation from chemical β-equilibrium e,p $\longleftrightarrow$ n^2. The chemical potentials include the rest mass of the species.

The ambipolar diffusion is then given as (Goldreich & Reisenegger 1992)

$$(\nabla\times B)\times B/4\pi=n_e\nabla(\Delta\mu)+n_e m_{\rm p}^{\star}\boldsymbol{v}/\tau_{\rm pn}, \tag{3}$$

where B is the core magnetic field and $m_{\rm p}^{\star}$ is the proton effective mass. The reaction rate is written as $dn_e/dt=-|\lambda\Delta\mu|$, where λ is related to the compressibility of the plasma and given by

$$\lambda\approx 5\times 10^{33}T_9^6(\rho/\rho_{\rm nuc})^{2/3}HQ_\lambda\ {\rm erg^{-1}\ cm^{-3}\ s^{-1}}. \tag{4}$$

Q_λ is the suppression of λ due to neutron superfluidity. H refers to the enhancement due to the deviation from β equilibrium.

Two regimes are possible: a friction-dominated regime where $l\gg a$ and a pressure pillow regime with $l\ll a$, where l is a characteristic scale of the field variation ΔB, and a is a characteristic length defined and given by Goldreich & Reisenegger (1992) as

$$a=(\tau_{\rm pn}n_e/\lambda m_{\rm p}^{\star})^{1/2}. \tag{5}$$

Further details are found in BL16.

2.2. Magnetar Heating by Ambipolar Diffusion

To calculate the ambipolar heating, we used (BL16)

$$dq_{\rm h}/dt\approx -B_{\rm l}^2 b(dl_{\rm l}/dt)/12\pi^2 \tag{6a}$$

where

$$dl_{\rm l}/dt\approx -\tau_{\rm pn}B_{\rm l}^2/(2\pi\rho_{\rm p}l_{\rm l})\quad {\rm for}\quad l_{\rm l}\geqslant l_\star, \tag{6b}$$

$$dl_{\rm l}/dt\approx -\lambda B_{\rm l}^2 l_{\rm l}/(4\pi n_e^2)\quad {\rm for}\quad l_{\rm l}\leqslant l_\star. \tag{6c}$$

Here $dq_{\rm h}/dt$ is the ambipolar heating rate, $l_{\rm l}$ is the characteristic size of the ambipolar heating region. $l_\star=l_{\rm l}$ when $l_{\rm l}=a\sqrt{2}$. $B_{\rm l}=2B_0/\pi$, where B_0 is the peak magnetic field in the core. Initially $B=B_0\sin bx$, and $l_{\rm l}$ and b are related by $l_{\rm l}=2/\pi b$.

Section 3.4 and the Appendix in BL16 give the details of their 1D (dimensional) model with the initial $B=B_0\sin bx$. Our simulation code is also 1D in the r direction. This (1D in the r direction) approach is essentially adopted in the "exact" thermal evolution code by the experts of this trade, since the variables and parameters change mostly in the r direction, not in the angular direction. If the magnetosphere is radial, the r direction flux in 1D is just multiplied by the whole surface area to obtain the total photon luminosity. In our current paper the dipole magnetosphere is adopted. Then, by integrating the 1D flux in each direction including the angular dependence of the dipolar field geometry, it was found that the net effect of the geometry is that the radial geometry case with the polar direction flux will be reduced by about 1/3. That is what our code does in this paper, to introduce the effect of magnetosphere geometry. For the 1D flux case we adopted the BL16 model explained in detail in that paper.

3. Magnetar Thermal Evolution Model

In our magnetar model, heating by the ambipolar diffusion under ultrastrong magnetic fields takes place in the central stellar core, while such ultrastrong magnetic fields also seriously alter the structure and properties of the surrounding crustal layers. By taking into account these new features, we constructed the thermal evolutionary simulation code for magnetars, revising the latest version of our exact evolutionary code for ordinary neutron stars.

Our neutron star evolutionary code has been developed over the years—for the details, see Nomoto & Tsuruta (1981, 1987), Tsuruta (1986, 1998, 2009), and Tsuruta et al. (2009). The set of general relativistic basic stellar structure evolution equations developed by Thorne (1977) is solved simultaneously from the stellar center to the surface without making isothermal approximations. The evolutionary simulation code was originally started by Nomoto & Tsuruta (1981, 1987) and has been continuously updated by adopting the most up-to-date microphysical input. See, e.g., Tsuruta (1998, 2009, 2018) and Tsuruta et al. (2009) for the details.

In the magnetar thermal evolutionary code constructed from the latest ordinary neutron star evolutionary code, the neutrino emissivity consists of all possible standard mechanisms, with the modified Urca, plasmon, pair neutrino, photoneutrino, bremsstrahlung, etc. The neutron superfluidity model with the critical temperature of $\log(T_{\rm crit}({\rm K}))=9.45$ (e.g., Tsuruta et al. 2009) is adopted. For the Cooper pair breaking and formation contribution, we found that many earlier publications, such as Yakovlev et al. (1999), give only incomplete treatments. Therefore, we took the more recent, updated version by Kolomeitsev & Voskresensky (2008). In addition, ambipolar heating 6(a) is adopted. In doing so, for the hotter earlier period, Equation 6(b) was used, while, during the later cooler period, Equation 6(c) was adopted.

This magnetar evolutionary simulation code was used for the evolution of the core from the center to the outer boundary chosen at $M_r=M_{\rm core}$ where the matter density ρ is as low as $\sim 10^9$ g cm^{-3}. (Here M_r is the baryon mass interior to the radius r.) With this code, we obtain the evolutionary change in the core temperature $T_{\rm core}$ at the outer boundary of $M_r=M_{\rm core}$.

For the EOS, the maximum mass of the neutron star has been found to be at least $2M_\odot$ (Demorest et al. 2010). Takatsuka et al. (2008) constructed an advanced EOS model, which we refer to as HP8u, with the maximum mass going beyond $2M_\odot$.

This model is based on the universal many-body interactions among both nucleons and hyperons (see Takatsuka et al. 2008; Tsuruta 2018 for the details). We used the HP8u EOS in our current work. For this EOS, the core of lower-mass, hotter stars consists mainly of neutrons and protons, while the major composition transforms to hyperons in heavier, cooler stars. The mass of the star at this transformation point is $1.45M_{\odot}$. Since magnetars should be hot, in this paper we adopt hotter, less-massive stars. Using the medium EOS HP8u (see, e.g., Tsuruta 2018 for the details of this EOS model), we constructed a neutron star model with $M = 1.4M_{\odot}$, where M is the total baryon mass of the neutron star (see Section 5.4 for the details). For this star, the central density is 1.0×10^{15} g cm^{-3}, and the radius is $R = 11.7$ km. We adopt the core mass, $M_{\rm core}$, for this model at $1 - M_{\rm core}/M = 4.7 \times 10^{-8}$, where $\rho_b = 2.0 \times 10^9$ g cm^{-3}.

For the envelope at $M_{\rm core} \leqslant M_r \leqslant M$, the spatially constant luminosity is a good approximation because of low densities. For the magnetar envelope, the ultrastrong magnetic fields significantly increase thermal conductivity in the crustal layers, which results in a significantly reduced difference between the core temperature and the surface temperature (Potekhin et al. 2015). BL16 calculated such magnetar envelope models and showed the results in their Figure 1. We approximate their relation between the core temperature, $T_{\rm core}$, and the surface photon luminosity, L_{γ}^{∞}, and obtained the following equations for four sets of B (3×10^{13} and 10^{15} G) and chemical composition (heavy element dominated such as Fe and light element contaminated).

For the $B = 10^{15}$ G and Fe case:

$$\log_{10}[L_{\gamma}^{\infty}(\text{erg s}^{-1})] = 1.96 \times \log_{10}[T_{\rm core}(\text{K})] + 17.446. \quad (7a)$$

For the $B = 3 \times 10^{13}$ G and Fe case:

$$\log_{10}[L_{\gamma}^{\infty}(\text{erg s}^{-1})] = 2.03 \times \log_{10}[T_{\rm core}(\text{K})] + 16.583. \quad (7b)$$

For the $B = 10^{15}$ G and light element case:

$$\log_{10}[L_{\gamma}^{\infty}(\text{erg s}^{-1})] = 1.50 \times \log_{10}[T_{\rm core}(\text{K})] + 21.869. \quad (7c)$$

For the $B = 3 \times 10^{13}$ G and light element case:

$$\log_{10}[L_{\gamma}^{\infty}(\text{erg s}^{-1})] = 1.50 \times \log_{10}[T_{\rm core}(\text{K})] + 21.673. \quad (7d)$$

These equations are good approximations of Figure 1 of BL16.

4. Results

Using the magnetar thermal evolutionary code as described in Section 3, the thermal evolution of six representative cases is calculated. The properties of these cases are shown in Table 1. B is the core magnetic field, and b is a parameter defined in Section 2. As a representative case we chose B to be $\sim 10^{16}$ G, because the earlier work (e.g., Heyl & Hernquist 1998) shows that for magnetars the core magnetic field will be about 10 times the surface magnetic field which is estimated to be about 10^{15} G. The first three are the cases adopted by BL16, while the last three are the additional choices with the different relevant combinations of B and b within the acceptable range.

The results for the six representative cases (see Table 1) are shown in Figure 2, where the core temperature versus age is shown. During the earliest stages the core temperature is too high ($T_{\rm core} \gtrsim 10^9$ K), for the heating to effectively compete with the neutrino cooling, and the star cools essentially by the escaping neutrinos. However, the heating becomes sufficient to balance cooling as the star cools down to around that temperature. Thereafter the curve follows the plateau region while cooling is balanced by heating. After the evolution reaches the characteristic time for the magnetic energy dissipation by this process (BL16), the curve goes down again, approaching the cooling curve.

The ultrastrong fields of magnetars also strongly affect the crustal layers from the radial position at $M_{\rm core}$ to the stellar surface, which significantly alters the relation between the core temperature and surface temperature. It depends on various microphysics of the crustal layers.

The most important is the composition. For instance, under the ultrastrong magnetar fields, thermal conductivity is much higher for light elements such as hydrogen, as compared with heavy elements (Potekhin et al. 2007). The dominant heavy element is Fe. But since magnetars are still relatively young, it is quite reasonable that the crusts are still contaminated by light

Table 1
Properties of the Six Representative Cases used in Figure 2

Model Name	B ($\times 10^{16}$ G)	b
BL16 (1)	1	$\pi \times 10^{-5}$
BL16 (2)	1.5	$\pi \times 10^{-5}$
BL16 (3)	1.5	10^{-6}
Case 4	0.7	$\pi \times 10^{-5}$
Case 5	0.8	10^{-6}
Case 6	0.8	$\pi \times 10^{-5}$

Note. The core magnetic field strengths B and the parameter b, as defined in Section 2, are shown for each case.

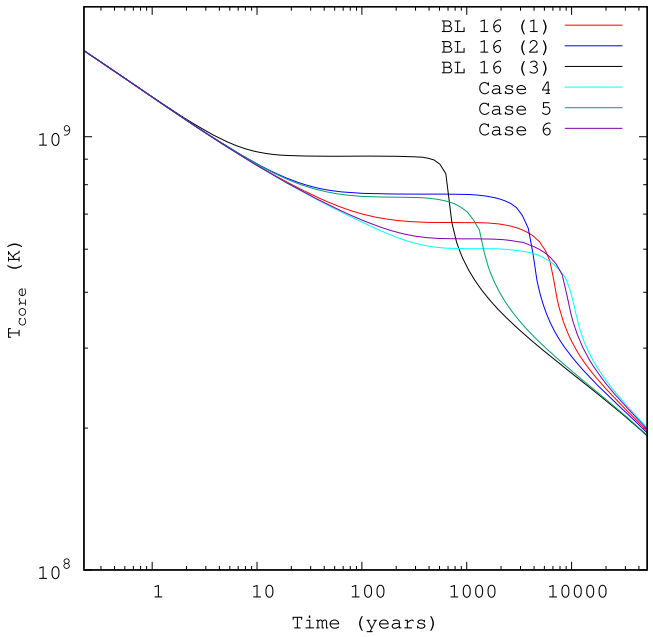

Figure 2. The core temperature vs. time from our simulations, for six representative cases in Table 1. The first three cases are the same as in BL16, to facilitate comparison with the BL16 curves. The last three choices are our own. See Table 1 for the details of the cases.

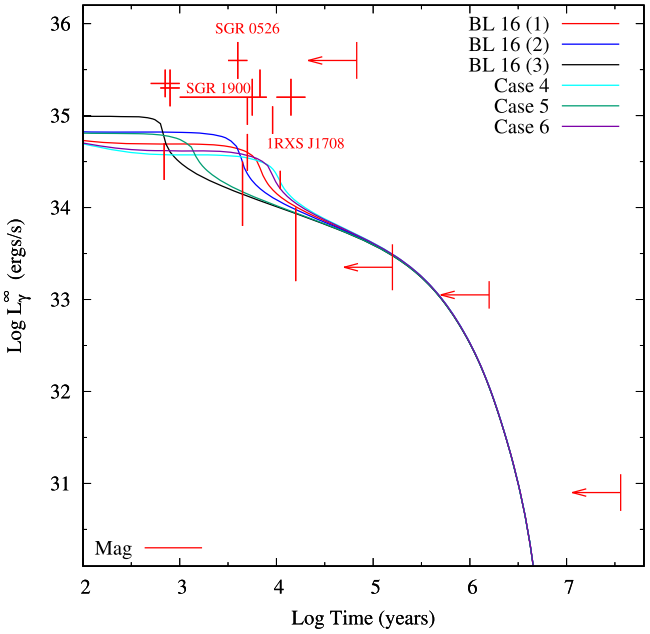

Figure 3. The thermal evolution of magnetars with ambipolar heating is compared with magnetar observation data. The six cases in Table 1 for models with the major crustal composition of Fe are shown as the surface photon luminosity vs. age. The bars and crosses are detections. The horizontal arrows are the upper limit to the age. The theoretical curves are consistent with cooler magnetar data.

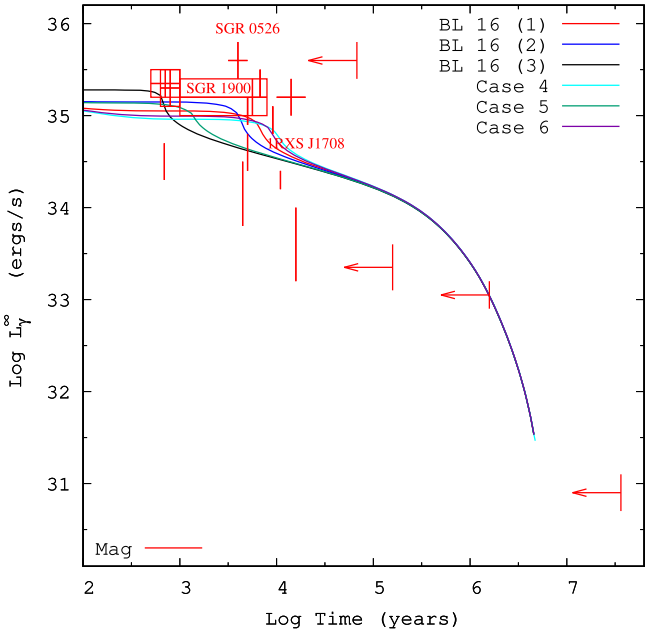

Figure 4. The same as Figure 3, except that the crustal layers of the star are now contaminated by light elements. The theoretical curves are now consistent with many hotter magnetar data. In this figure, to avoid overcrowding, only the 1σ errors are shown. When 3σ errors are included, the data points of only a few hottest sources are still off the curves.

elements in some cases. Equations 7(a)–(d) show the surface radiation as a function of core temperature for both cases, with two representative surface magnetic field strengths of 10^{15} G and 3×10^{13} G.

For the six representative cases in Table 1, thermal evolution (cooling and heating) curves are shown, as the surface photon luminosity versus age relation for the Fe envelope case in Figure 3, while the case for the light element contaminated envelope is shown in Figure 4. The surface magnetic field used is 10^{15} G. For comparison the observed surface luminosity data of various magnetars with different ages, taken from Viganò et al. (2013), are also shown.

First consider the evolution of the central temperature. Our core temperature versus age relation is shown in Figure 2 for the six representative cases in Table 1. Similar core temperature evolution for the isothermal model was obtained by BL16 for the top three cases of our Table 1, and that is shown in their Figure 3. Comparing Figure 3 of BL16 and our Figure 2, qualitatively it may appear that the effect of the ambipolar heating on the core temperature evolution is similar between their isothermal model and our model. However, some important differences are noted.

For instance, in our case the curves are generally more smooth, especially during the decaying stages. In our model the transition from the earlier to the later period is smooth, not abrupt. More importantly, the plateau and decaying phases in our case are more gradual and longer (compare their Figure 3 and our Figure 2). That makes the temperature higher in our model during the decaying phase. That is important because that is the critical location of most observed temperature data.

Now we consider the thermal evolution behavior expressed as the evolution of the surface photon luminosity (and hence the surface temperature) versus age. We calculated the surface temperature evolution for $B = 10^{15}$ G, and the results are shown in Figures 3 and 4. Figure 4 shows that in the light element case the surface temperature becomes significantly higher. Compare Figures 3 and 4. Note that the Fe envelope case (Figure 3), where the temperature is lower, still agrees with cooler observed data, but not some hotter ones. On the other hand, in Figure 4 with the light element case, due to the higher surface temperature, theoretical curves cover more higher temperature observed data. In this figure, to avoid overcrowding, only the 1σ errors are shown. When 3σ errors are included, the data points of only a few hottest sources are still off the curves.

Here the major reasons are summarized: First of all, the star still cools with escaping neutrinos from the core for magnetars due to their relatively younger ages, and hence the evolution is determined by the core temperature. For the same core temperature, the surface temperature is higher in the light element case than the case with only heavy elements due to the enhanced crustal thermal conductivity for light elements with ultrastrong field magnetars.

In conclusion, combining Figure 3 for the Fe crust case and Figure 4 for the light element contaminated case, the observed magnetar temperature data can mostly agree with the theoretical predictions from the ambipolar heating.

5. Discussion

5.1. Comparison with Earlier Work

BL16 did not convert their core temperature evolution results (shown in their Figure 3) to the surface temperature evolution case. Instead, these authors converted the observed surface temperature data to the corresponding core temperature data in their Figure 3, shown as a green box. By comparing that with their core temperature evolution curves, it is noted that the observed temperature is too high for their ambipolar heating scenario, because the green box lies above their ambipolar

heating curves. The reason is that when these authors converted the observed surface temperature data to the core temperature data, they did not include the light element contaminated crust case. If they had done so, the lower end of their green box would have gone down considerably, getting closer to their heating curves. Their abstract does note that if the light element case is included, the observed data are consistent with the ambipolar heating. By examining BL16's Figure 1 where the surface radiation versus core temperature relations are shown, it is clear that for the same surface luminosity (and hence surface temperature), the corresponding core temperature should be significantly lower for the light element case (the red curves) than the Fe cases (blue curves) in their Figure 1. That means the bottom of the green box in their Figure 3 should be much lower when the light element case is included.

Another significant difference is that BL16 adopted the modified Urca (their Murca) alone, while our neutrino emission includes the effects of neutron superfluidity. The Cooper pair breaking and formation contribution, which we included, increases the neutrino emission immediately below the critical temperature $T_{\rm crit} = 10^{9.45}$(K). However, this Cooper pair emission decreases rapidly to below the superfluid suppressed case, which is below the Murca alone case. By the time the core temperature reaches the typical temperatures of the magnetars, at around 3×10^8 K, the neutrino emission is significantly below the Murca alone case. See, e.g., Figure 2 of BL16, where a similar neutron superfluid model (red curves) is shown. Due to our overall reduced neutrino emission at around the age of magnetars, our heating lasts longer.

Another reason for the difference between BL16 and our results is that when we adopt our more realistic numerical evolutionary simulation code, the decaying phase of the heating curve is more gradual, not abrupt, which happens in the BL16 case. (Compare their Figure 3 and our Figure 2.) That also results in the surface temperature of our model being higher for longer periods during the decaying phase where most of the magnetar observational data are located.

5.2. Effects of Neutron Superfluidity

$Q_{\rm pn}$ describes suppression of the rate of collisions among protons and neutrons. We set $Q_{\rm pn} = 1$ for the effect of neutron superfluidity on the ambipolar heating since numerical information is not available. However, we investigated its qualitative net effect to our results, and reached the following conclusion: Heating rate $dq_{\rm h}/dt$ in Equation 6(a) is proportional to dl_1/dt, which goes as $\tau_{\rm pn}$ (Equation 6(b)). $\tau_{\rm pn}$ goes as $1/Q_{\rm pn}$ (Equation (1)). With superfluidity, $Q_{\rm pn} < 1$. Then $\tau_{\rm pn}$ is larger with superfluidity. Then, ambipolar heating $dq_{\rm h}/dt$ gets higher because it goes as dl_1/dt (Equation 6(a)), which goes as $\tau_{\rm pn}$ (Equation 6(b)). That means the ambipolar heating will increase with neutron superfluidity. (Note that BL16 also reached the same conclusion.) Therefore, if neutron superfluid is included in our heating calculations, heating will increase. That means heating will last longer, and our final conclusion on the validity of the ambipolar heating will become even stronger.

5.3. Effects of Proton Superconductivity

The effect of superconductivity should be considered if the field $B < H_{c2}$ (Sinha & Sedrakian 2015, here referred to as Sinha15). For our neutron star model, the central density ρ_c is 10^{15} gm cm^{-3}. Table 1 in Sinha15 shows that for that density, $H_{c2} < 0.03(\sim 3 \times 10^{14}$ G). Since our core $B \sim 10^{16}$ G $\gg H_{c2}$ in the central core, the effect of superconductivity should be negligible. Note that H_{c2} depends on density. BL16 also note that superconductivity is negligible for magnetars. (Near the core boundary, the density drops to near the nuclear density and then $H_{c2} > 10^{16}$ G (see Sinha15, Table 1), but the neutron star core is almost constant density. Therefore the volume where the density drops to the nuclear density region near the core boundary is negligible compared with the whole core volume. Therefore, the contribution from near the edge of the core is negligible.)

5.4. Effects of Stellar Model

When the stellar mass gets beyond 1.45 $M_\odot$, our EOS model includes hyperons. Our current paper tests if a magnetar model CAN get hot enough to be consistent with the observed magnetar data with the ambipolar heating. We showed, for the low-mass 1.4 $M_\odot$ star, that is yes. With the EOS we adopted (which is perfectly relevant), this happens to be still a neutron star. Hyperon-mixed stars are heavier and cooler, and with our EOS model it is harder to heat more massive and cooler hyperon-mixed stars enough to the level of many of the observed hotter magnetar data. We showed that, at least for less-massive stars (which in our model happens to have no hyperons), this high heating is possible. In some other relevant EOS models where transformation to hyperons takes place at lower density and mass (e.g., Raduta et al. 2018), low-mass stars may already contain hyperons. For these stars the same conclusion applies. Whether hyperons are present or not is not the issue in our current particular problem. It shows that, at least for lower-mass hotter stars, the ambipolar heating is consistent with most of the observed magnetar data.

6. Conclusions

We investigated the possibility of ambipolar heating in the stellar core as the source of magnetar's high temperatures. Our results are:

(i) If both the heavy element crust case and the light element contaminated crust case are considered, the ambipolar heating can be consistent with most of the observed magnetar temperatures.
(ii) If neutrons are in the superfluid state, the ambipolar heating increases, and the heating phase can last longer to be consistent with the observed magnetar temperatures (see Section 5.2).
(iii) The adoption of the relativistic thermal evolution simulation code with a realistic magnetar model results in the evolution becoming more smooth and gradual. That helps higher temperatures during the decaying phase.

By adopting an isothermal, nonrelativistic model with an analytic approach, BL16 predicted that, if the stellar crust is contaminated by light elements and the core magnetic field can be as strong as 10^{16} G, the ambipolar heating may heat the magnetars to the observed temperatures. At the same time, these authors pointed out that such a high-temperature phase may not last long enough.

Our results mostly confirm their estimates. However, it may be pointed out that the magnetars may last long enough especially if the neutrons in the interior are in a superfluid state, which is quite possible. Also it is quite possible that the

magnetic field in the interior can be as high as 10^{16} G (e.g., see Heyl & Hernquist 1998; Potekhin et al. 2015). Also it is quite reasonable that magnetars still contain light elements due to their relatively young age.

Our conclusion is that the ambipolar heating can be consistent with the observed high temperature of magnetars.

We thank the referee for constructive suggestions and comments. This work has been supported by the Kavli IPMU and the World Premier International Research Center Initiative (WPI), MEXT, Japan, and the Japan Society for the Promotion of Science (JSPS) KAKENHI grants JP17K05382, JP20K04024, JP21H04499, and JP21K20369.

ORCID iDs

Ken'ichi Nomoto https://orcid.org/0000-0001-9553-0685

References

Beloborodov, A. M., & Li, X. 2016, ApJ, 833, 261
Demorest, P. B., Pennucci, T., Ransom, S. M., Roberts, M. S. E., & Hessels, J. W. T. 2010, Natur, 467, 1081
Goldreich, P., & Reisenegger, A. 1992, ApJ, 395, 250
Heyl, J. S., & Hernquist, L. 1998, MNRAS, 300, 599
Kaminker, A. D., Yakovlev, D. G., Potekhin, A. Y., et al. 2006, MNRAS, 371, 477
Kolomeitsev, E. E., & Voskresensky, D. N. 2008, PhRvC, 77, 065808
Mereghetti, S. 2008, A&ARv, 15, 225
Nomoto, K., & Tsuruta, S. 1981, ApJL, 250, L19
Nomoto, K., & Tsuruta, S. 1987, ApJ, 312, 711
Potekhin, A. Y., Chabrier, G., & Yakovlev, D. G. 2007, Ap&SS, 308, 353
Potekhin, A. Y., Pons, J. A., & Page, D. 2015, SSRv, 191, 239
Raduta, A. R., Sedrakian, A., & Weber, F. 2018, MNRAS, 475, 4347
Sinha, M., & Sedrakian, A. 2015, PhRvC, 91, 035805
Takatsuka, T., Nishizaki, S., Tamagaki, R., et al. 2008, in AIP Conf. Ser. 1011, New Facet of Three Nucleon Force—50 Years of Fujita Miyazawa, ed. H. Sakai, K. Sekiguchi, & B. F. Gibson (Melville, NY: AIP), 209
Thompson, C., & Duncan, R. C. 1996, ApJ, 473, 322
Thompson, C., & Duncan, R. C. 2001, ApJ, 561, 980
Thorne, K. S. 1977, ApJ, 212, 825
Tsuruta, S. 1964, PhD thesis, Columbia Univ.
Tsuruta, S. 1979, PhR, 56, 237
Tsuruta, S. 1986, ComAp, 11, 151
Tsuruta, S. 1998, PhR, 292, 1
Tsuruta, S. 2009, in Neutron Stars and Pulsars, Astrophysics and Space Science Library, ed. W. Becker, Vol. 357 (Berlin: Springer), 289
Tsuruta, S. 2018, in Fourteenth Marcel Grossmann Meeting—MG14, ed. M. Bianchi, R. T. Jansen, & R. Ruffini (Singapore: World Scientific), 160
Tsuruta, S., Sadino, J., Kobelski, A., et al. 2009, ApJ, 691, 621
Viganò, D., Rea, N., Pons, J. A., et al. 2013, MNRAS, 434, 123
Yakovlev, D. G., Kaminker, A. D., & Levenfish, K. P. 1999, A&A, 343, 650